

[Click here to view linked References](#)

Plasmonics manuscript No.
(will be inserted by the editor)

Tuning of SPR for colocalized characterization of biomolecules using nanoparticle-containing (multi)layers

Jan Dvořák¹ · Ondřej Caha^{1,2} ·
Dušan Hemzal^{1,2}

Received: date / Accepted: date

Abstract In this contribution we quantify the fine-tuning of surface plasmon resonance via nanoparticle coating of gold SPR chips. We target preparation of atomically flat surface with defined charge, needed for scanning probe characterization of biomolecules, with simultaneous optimization of in situ SPR sensitivity during immobilization of these molecules. Using Total internal reflection ellipsometry we show that the goal can be achieved by combination of charge-stabilized silver nanoparticles over underlying gold chip of reduced thickness. The provided formulas for optimal silver to gold thickness relation are valid for arbitrary analyte and the method was experimentally verified on binding of Rtt103 protein.

Keywords SPR, TIRE, nanoparticles, Rtt103

Introduction

Scanning probe characterization of biomolecules such as DNA or proteins requires atomically flat substrates. Usually, freshly cleaved mica is used with AFM, while for STM one needs a conductive substrate such as highly oriented pyrolytic graphite (HOPG). As a solution, one may coat mica or graphite with thin metallic overlayer. However, surface flatness of such layers is far from atomic. The situation is only partially improved using additional treatment of the substrate such as flame annealing [1], although template stripping [2] seems promising even for large area surfaces.

In addition to topographical imprint, a thin bio-molecular film adsorbed on the substrate also produces small changes in the measured optical spectra. When silver or gold are used for substrate coating, surface plasmon resonance (SPR) can be achieved [3], enhancing substantially sensitivity of the optical characterization. Although silver exhibits stronger enhancement, gold is usually preferred thanks to its bio-compatibility and inert nature. As a remedy, multilayers containing both metals have been suggested [4] leading to high sensitivity due to silver interlayer,

¹ Dept. condensed matter physics, Masaryk university, Brno, Czech Republic

² CEITEC, Masaryk university, Brno, Czech Republic
corresponding author : Dušan Hemzal, E-mail: hemzal@physics.muni.cz

yet isolating it from direct contact with sample by a thin gold capping. However, the problems with surface quality persist.

Luckily, it is possible to grow sufficiently large flat nanoparticles, whose facets are perfect crystallographic planes [5]. In this regard, gold nanoplates with triangular shape have been suggested as a convenient tip-enhanced Raman substrate [6]. Moreover, nanoparticles are usually produced already capped to retain charge or steric stabilization. This allows to use the strong resonance of silver for tuning the sensitivity of bare gold chip towards growing biomolecular layers without need for additional over-layers.

Concerning optical constants of the noble metal layers at nanoscale, the free electron contribution to dielectric function is influenced by collisions at nanoparticle boundaries leading to change of the damping constant γ in the Drude formula. Using the results of Ref. [7], the bulk dielectric function $\varepsilon_{\text{bulk}}$ is modified to $\varepsilon_{\text{nano}}$ via

$$\varepsilon_{\text{nano}} \doteq \varepsilon_{\text{bulk}} - \left(\frac{\omega_p^2}{\omega^2 + i\omega\gamma_{\text{nano}}} - \frac{\omega_p^2}{\omega^2 - i\omega\gamma_{\text{bulk}}} \right), \quad (1)$$

where ω_p is the (bulk) plasma frequency and the nanoscale-corrected damping factor γ_{nano} reads

$$\gamma_{\text{nano}} = \gamma_{\text{bulk}} + \sigma \frac{v_F}{a},$$

with γ_{bulk} the bulk damping, a the radius of the nanoparticle and v_F the velocity of electrons at Fermi level; the value of σ depends on the character of the collision processes.

Sample nano-corrected optical constants of bulk silver are shown in Fig. 1; for thicknesses below 10 nm, the correction is significant.

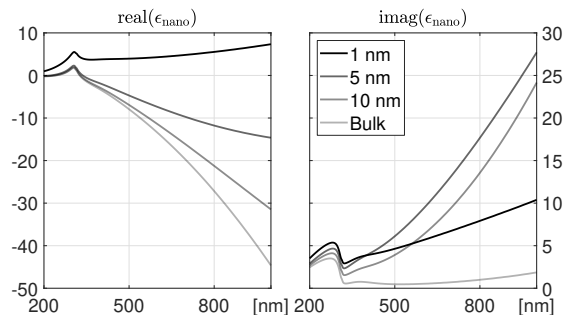


Fig. 1 Optical constants of a thin silver film calculated from [8] using nanoscale correction (1) for different thicknesses of the film (dark to light traces).

The SPR analysis is usually performed using angle-scanned reflectivity of the samples in the total internal reflection (TIR) setting. However, combining SPR with spectroscopic ellipsometry [9] results in SPR-TIRE [10], which surpasses conventional SPR measurement in sensitivity thanks to additional information on the reflection induced phase-shifts [11]; see Fig. 2 for a schematic setup.

In brief, substrate spectra of the ellipsometric angles Ψ and Δ exhibit characteristic behavior near SPR: Ψ (connected with the commonly measured reflectivity of the substrate) shows a dip, while Δ (bringing additional information on the phase change) shows a jump. During immobilization of analyte the SPR dip acquires primarily a slight shift. The resulting change in ellipsometric angles will be highest at wavelengths near the steepest points in the substrate spectra. Hence, maximum derivatives Ψ'_{\max} , Δ'_{\max} of the substrate ellipsometric angles constitute a convenient measure of the sensitivity.

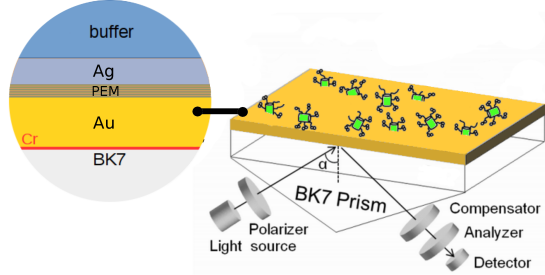


Fig. 2 In SPR-TIRE, analyte is transported to the active surface of an SPR chip using microfluidic setup. Amplitude and phase of light (totally) reflected from the chip are measured through a coupling prism using ellipsometric setup. Adapted from [12].

The properties of TIRE (in accordance with common practice, we will omit the prefix SPR) spectra are demonstrated in the top panel of Fig. 3 for a simple layered system in water ambient; the overall quality of the resonance is linked to the sharpness of the SPR dip in Ψ (upper panel). Starting from a substrate with bare gold layer of optimal thickness, an addition of a silver layer shifts the system off resonance and the sensitivity decreases. Consequently, with multilayer substrates one should start with a thinner (off-resonance) gold layer so that the added silver layer shifted the system to optimal resonance and recovered its sensitivity with respect to further immobilization of the biomolecules.

In this way, optimal resonance of gold chips can be tuned using silver nanoparticles. To this end, we first establish optimal relation between gold and silver thickness in the next section. Consequently, silver nanoparticles are synthesized and attached via polyelectrolyte multilayer to a fitting gold chip. In the final step, a selected protein is immobilized over the nanoparticles. All deposition steps have been monitored in situ using TIRE.

Theory

To model the sensitivity of a TIRE measurement, we use the matrix formalism: in a layered structure with planar interfaces, the incident (E_i), reflected (E_r) and transmitted (E_t) wave amplitudes of the propagating electric field are connected through

$$\begin{bmatrix} E_i \\ E_r \end{bmatrix} = \mathbf{V}_0^{-1} \mathbf{R}_1^{-1} \dots \mathbf{R}_m^{-1} \mathbf{V}_f \begin{bmatrix} E_t \\ 0 \end{bmatrix} \equiv \mathbf{P} \begin{bmatrix} E_t \\ 0 \end{bmatrix}, \quad (2)$$

where matrices \mathbf{R}_j , $j = 1 \dots m$, belong to j -th layer of the structure and matrices \mathbf{V} are connected with substrate (denoted from now on with subscript $_0$) and ambient (subscript $_f$). The resulting components of the overall propagation matrix \mathbf{P} are polarization-dependent, we will also use subscripts to distinguish the two polarizations,

$$p: \mathbf{P} \equiv \begin{pmatrix} a_p & b_p \\ c_p & d_p \end{pmatrix}, \quad s: \mathbf{P} \equiv \begin{pmatrix} a_s & b_s \\ c_s & d_s \end{pmatrix}.$$

Rather than evaluating the substrate angles Ψ_0 , Δ_0 and than going for cumbersome calculation of their derivative, we will analyze the difference spectra $\bar{\Psi} \equiv \Psi - \Psi_0$, $\bar{\Delta} \equiv \Delta - \Delta_0$ between substrate measurement yielding Ψ_0 , Δ_0 and sample measurement yielding Ψ , Δ . From experimental point of view, difference spectra significantly improve visualization of the small changes caused by the involved thin films by suppressing the SPR background common to sample and substrate measurement (see Fig. 3). From theoretical point of view, we take advantage of the closed form of the difference spectra that we have provided earlier [12]: a thin overlayer with thickness t and index of refraction n introduces changes

$$\Psi - \Psi_0 \approx 2\pi \text{Im} \left\{ \frac{F}{F_0} - \frac{E}{E_0} \right\} \frac{|\rho_0|}{1 + |\rho_0|^2} \frac{t}{\lambda}, \quad (3)$$

$$\Delta - \Delta_0 \approx -2\pi \text{Re} \left\{ \frac{F}{F_0} - \frac{E}{E_0} \right\} \frac{t}{\lambda}, \quad (4)$$

where $\rho_0 = F_0/E_0$ is the complex reflectance ratio of the substrate and F , F_0 , E , E_0 are polarization dependent functions of the propagation matrix components, eg. $F_0 = c_{0p}a_{0s}$, $E_0 = a_{0p}c_{0s}$ etc, where zero in subscript denotes substrate values; for a complete introduction of the matrix formalism and difference spectra see Supplement.

Obtainable directly from substrate and sample measurements, the difference spectra (3), (4) constitute a measurement-based alternative to derivative of the substrate ellipsometric angles. As such, we will study in particular the difference spectrum in Δ because of its feasibility: monitoring Δ brings higher sensitivity than Ψ [13] and, in addition, $\Delta - \Delta_0$ exhibits an isolated peak near SPR resonance, which favors its detection. The higher the magnitude $\bar{\Delta}_{\text{max}}$ of this peak, the better the sensitivity.

By inspection of (4) one finds that $F_0 \rightarrow 0$ near resonance, producing the major contribution to $\bar{\Delta}_{\text{max}}$. As a matter of fact, it is only c_{0p} which goes to zero in the denominator of F_0 . This is not surprising since c_{0p} is the component of \mathbf{P} responsible for vanishing of p-polarized reflectivity near resonance.

We will use a two-layer model of a thin silver overlayer with index of refraction n_{Ag} and thickness t_{Ag} over a gold layer with index of refraction n_{Au} and thickness t_{Au} . The angles of propagation of light within silver and gold layer are φ_{Ag} and φ_{Au} , respectively. Thus, in our case the overall propagation matrix reads $\mathbf{P}_0 = \mathbf{V}_0^{-1} \mathbf{R}_{\text{Au}}^{-1} \mathbf{R}_{\text{Ag}}^{-1} \mathbf{V}_f$.

Consequently, to prepare chips with optimal sensitivity we will seek the extreme of c_{0p} in dependence on thicknesses t_{Au} and t_{Ag} . In this way, the results will lie close to those obtainable from the substrate spectra derivatives. In addition, use of c_{0p} , which is connected only with substrate, is advantageous as the obtained results will be independent of the analyte.

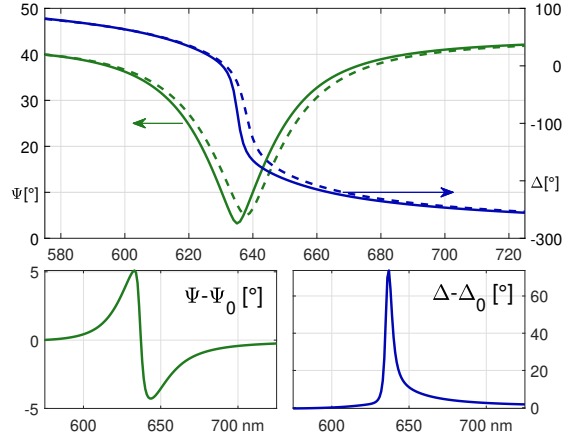


Fig. 3 Simulation of ellipsometric spectra for substrate with 47 nm of Au (dashed lines) and after its covering with 1 nm of Ag (full lines). Top panel: spectral dependence of Ψ (green) and Δ (blue), bottom panels: difference spectra in Ψ and Δ .

Concerning approximation of the optical path¹, the considered thickness t_{Ag} is small enough to allow the linear expansion $\mathbf{R}_{\text{Ag}}^{-1} \doteq \mathbf{I} - \delta\mathbf{S}t_{\text{Ag}}$, where

$$\delta\mathbf{S} = \begin{pmatrix} 0 & i \frac{\cos \varphi_{\text{Ag}}}{n_{\text{Ag}}} \\ i \frac{n_{\text{Ag}}}{\cos \varphi_{\text{Ag}}} & 0 \end{pmatrix} \tilde{\theta}_{\text{Ag}}, \quad (5)$$

with $\tilde{\theta}_{\text{Ag}} = (2\pi/\lambda_0)n_{\text{Ag}} \cos \varphi_{\text{Ag}}$ for the vacuum wavelength λ_0 .

For gold, the situation is somewhat different: there is an optimal thickness t_{opt} of (bare) gold, which will be only slightly changed by the addition of silver. Hence, we can assume $t_{\text{Au}} = t_{\text{opt}} + \delta t$ and after expansion for small δt obtain $\mathbf{R}_{\text{Au}}^{-1} \doteq \mathbf{R}_{\text{opt}}^{-1} - \delta\hat{\mathbf{S}}\delta t$, where

$$\mathbf{R}_{\text{opt}}^{-1} = \begin{pmatrix} \cos \theta_{\text{opt}} & -i \frac{\cos \varphi_{\text{Au}}}{n_{\text{Au}}} \sin \theta_{\text{opt}} \\ -i \frac{n_{\text{Au}}}{\cos \varphi_{\text{Au}}} \sin \theta_{\text{opt}} & \cos \theta_{\text{opt}} \end{pmatrix} \quad (6)$$

is the propagation matrix for bare gold of the optimal thickness and

$$\delta\hat{\mathbf{S}} = \begin{pmatrix} \sin \theta_{\text{opt}} & i \frac{\cos \varphi_{\text{Au}}}{n_{\text{Au}}} \cos \theta_{\text{opt}} \\ i \frac{n_{\text{Au}}}{\cos \varphi_{\text{Au}}} \cos \theta_{\text{opt}} & \sin \theta_{\text{opt}} \end{pmatrix} \tilde{\theta}_{\text{Au}}, \quad (7)$$

where $\tilde{\theta}_{\text{Au}} = (2\pi/\lambda_0)n_{\text{Au}} \cos \varphi_{\text{Au}}$ and $\theta_{\text{opt}} = \tilde{\theta}_{\text{Au}}t_{\text{opt}}$.

To isolate c_{0p} from \mathbf{P}_0 one can introduce an auxiliary vector

$$\mathbf{c}_{0p} \equiv \begin{pmatrix} 0 \\ c_{0p} \end{pmatrix} = \begin{pmatrix} 0 & 0 \\ 0 & 1 \end{pmatrix} \mathbf{V}_0^{-1} \mathbf{R}_{\text{Au}}^{-1} \mathbf{R}_{\text{Ag}}^{-1} \mathbf{V}_f \begin{pmatrix} 1 \\ 0 \end{pmatrix},$$

¹ Since we are to work with p-polarized light exclusively, we will mostly omit the polarization distinguishing indexes for brevity.

whose module provides the amplitude of c_{0p} : $\mathbf{c}_{0p} \cdot \mathbf{c}_{0p} = |c_{0p}|^2$, where the scalar product is defined in matrix formalism using the Hermite conjugate. Denoting

$$\tilde{\mathbf{V}}_0^{-1} \equiv \begin{pmatrix} 0 & 0 \\ 0 & 1 \end{pmatrix} \mathbf{V}_0^{-1} \quad \mathbf{v}_f \equiv \mathbf{V}_f \begin{pmatrix} 1 \\ 0 \end{pmatrix},$$

and using the above expansions (5)-(7), one can write

$$\mathbf{c}_{0p} \doteq (\mathbf{k} - \mathbf{l}t_{Ag}) - (\mathbf{m} - \mathbf{n}t_{Ag})\delta t, \quad (8)$$

where $\mathbf{k} = \tilde{\mathbf{V}}_0^{-1} \mathbf{R}_{opt}^{-1} \mathbf{v}_f$, $\mathbf{l} = \tilde{\mathbf{V}}_0^{-1} \mathbf{R}_{opt}^{-1} \delta \mathbf{S} \mathbf{v}_f$, $\mathbf{m} = \tilde{\mathbf{V}}_0^{-1} \delta \hat{\mathbf{S}} \mathbf{v}_f$ and $\mathbf{n} = \tilde{\mathbf{V}}_0^{-1} \delta \hat{\mathbf{S}} \delta \mathbf{S} \mathbf{v}_f$. To obtain the sought for dependence $\delta t(t_{Ag})$ we find an extreme of $|c_{0p}|^2$ through derivative w.r.t. δt . Using (8), one obtains

$$\delta t \doteq \frac{\text{Re}\{(\mathbf{k} - \mathbf{l}t_{Ag}) \cdot (\mathbf{m} - \mathbf{n}t_{Ag})\}}{|\mathbf{m} - \mathbf{n}t_{Ag}|^2}, \quad (9)$$

which is a ratio of two polynomials, each quadratic in t_{Ag} .

Without silver, optimal bulk thickness of gold must be preserved. Using $t_{Ag} = 0$ in (9), the subsequent requirement $\delta t = 0$ allows to find t_{opt} for selected wavelength and given optical constants of gold through $\text{Re}\{\mathbf{k} \cdot \mathbf{m}\} = 0$; for further details on the whole derivation see Supplement.

Measurement

During binding of the biomolecules, their surface charge plays the crucial role. For example, DNA exhibits negative charge from phosphate backbone and will, hence, require a positively charged surface or linker to bind [14]. On the other hand, proteins carry local surface charges depending on their secondary structure through the amino acid side chains.

In our previous work [12] we reported on TIRE measurement of weak ($K_d \approx 10^{-3}$ M) protein-protein interaction between carboxy-terminal domain (CTD) of RNA polymerase II (RNAPII) and CTD-interaction domain (CID) of Rtt103 protein, one of RNAPII co-transcriptional factors [15]. Although transcription of DNA by RNAPII is essential during gene expression, there are only few structures available for processing factors bound to the modified CTD [16] because this weak interactions are undetectable by most biochemical methods. Fortunately, SPR techniques including TIRE constitute a feasible alternative [17].

Rendering the surface of Rtt103-CID prevalently positive, the elevated arginine content makes the protein a good candidate for binding to the wide-spread citrate stabilized nanoparticles, which combine negative surface charge with excellent stability for both gold [18] and silver [19]. Consequently, a positively charged binding layer will be required over the gold chip to immobilize these nanoparticles. To study the optimal conditions for SPR in detail, we will investigate gold chips with gradient of thickness.

Experimental. Gold layers were deposited on clean BK7 slides by PVD with thickness gradient along one direction of the chip. They were coupled to a semi-cylindrical BK7 prism using immersion oil. Ellipsometric angles Ψ , Δ were recorded during the binding experiment with Woollam VASE ellipsometer in the spectral range 450–750 nm using auto-retarder and focussation probes at room temperature. The TIRE microfluidic transport system consisted of a

disposable home-made liquid cell with 1 mm x 20 mm channel of thickness 200 μm , a 480 μl degasser to remove residual gas in the liquid, and a syringe pump to control the liquid flow rate. The chips were loaded into the liquid cell in Kretschmann configuration with gradient of gold thickness along the microfluidic channel. After thorough washing with water, optimal resonance curves were found for AOI 74° at a certain position along the gold thickness gradient. Next, a poly(ethylenimine) (PEI) self-organized monolayer (SAM) was created on the surface of the chip to facilitate subsequent immobilization of citrate-stabilized silver nanoparticles (AgNP) of triangular shape. Finally, the Rtt103 protein was bound over AgNP.

The UV-VIS spectra were acquired using Varian Cary 5e spectrometer and SPM characterization was performed using NT-MDT Ntegra Spectra. The X-ray reflectivity was measured using Rigaku SmartLab diffractometer equipped with copper X-ray tube; the beam size was 1 mm x 2 mm.

For details on substrate preparation and chemistry involved, see Appendix.

The gold layer with gradient thickness was designed with optimal SPR near the thick side of the chip. After PVD coating, the BK7/Au substrates were characterized using X-ray reflectivity, showing dense layer of gold with a possibly formed interlayer at the contact with BK7 (see Supplement for more details). The obtained thickness range 27-41 nm with linear gradient 0.6 nm/mm along the whole chip was used to calibrate the measured UV-VIS spectra.

The silver nanoparticles were synthesized according to [20]. The halide presence during synthesis produces selectively etched triangular prisms; lateral size about 60 nm and thickness about 5 nm were targeted.

To create a charged surface of the SPR chip, we use the PEI-PSS-PAH polyelectrolyte multilayer. The system is thoroughly understood [21,22] including TIRE studies [23]. To achieve positively charged surface, single coating with PEI was used.

The results of TIRE measurement on AgNP activated chips with gradient of gold thickness are shown in Fig. 4. The figure summarizes the final two steps of the experiment: measurement of BK7/Au/PEI/AgNP substrate (dashed traces) and its coating with Rtt103-CID (solid traces). Several spectra along the microfluidic channel were taken (dark to light traces) relative to location of optimal resonance on bare gold. In all cases, coating with protein caused small, but measurable changes in the spectra (top row). To visualize these changes, the figure shows for comparison derivative of the substrate spectra (center row) and the difference spectra between the protein-coated and bare substrate (bottom row). Coalescing the peak of the difference spectrum $\Delta - \Delta_0$ and maximum substrate derivative Δ'_0 , the figure Fig. 4 confirms equivalence of the two treatments.

Finally, AFM characterization of a generic substrate after individual deposition steps is presented in Fig. 5. The initial roughness of polished glass below 1 nm is corrupted by PVD deposition of gold. Subsequently, the surface is slightly smoothed by PEI. In the last step, nanoparticles bind through their negative charges to the positive polymer with surface coverage about 5%. The shown height profile (bottom panel) confirms expected thickness of the nanoparticles.

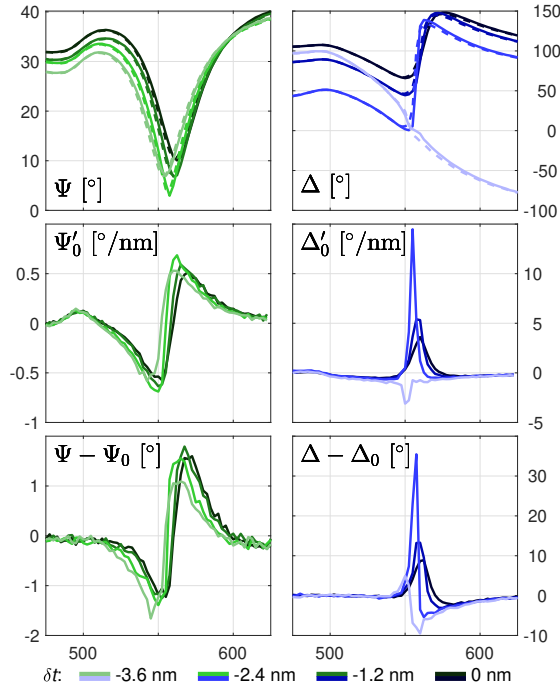


Fig. 4 Evaluation of TIRE sensitivity at $\text{AOI} = 74^\circ$; measured spectra (top row) of BK7/Au/PEI/AgNP substrate before (dashed) and after immobilization of Rtt103-CID (solid) and comparison of substrate spectra derivative (central row) and the sample difference spectra (bottom row). The individual traces correspond to different places along the chip, as denoted in the legend using δt relative to optimal thickness of bare gold. Note the different vertical scale in the panels.

Results and Discussion

The results of the sensitivity modelling of the silver coated gold chip using bulk optical constants of gold from [24] and those of silver from [8] are shown in the Supplement. Although prediction by the approximate formula (9) follows reasonably the full numerical simulations, the obtained values for thickness correction of gold disagree with the measurements presented in Fig. 4 by an order of magnitude and the situation does not improve significantly after using of nanoscale-corrected optical constants of silver.

Atop correction to nanoscale, one has to distinguish between effective thickness of the whole silver layer and thickness of the nanoparticles themselves. This is the role of effective medium. In our case, the chosen approximation must also comprise the resonant character of silver. To this end, we will use the Bruggeman's approximation [25]: for inclusion of quasi-spherical particles with permittivity ε_b with mixing ratio $0 \leq f_b \leq 1$ in medium with ε_a the permittivity ε_{eff} of the effective medium solves equation

$$2\varepsilon_{\text{eff}}^2 + \varepsilon_{\text{eff}} [(3f_b - 2)\varepsilon_a + (1 - 3f_b)\varepsilon_b] - \varepsilon_a\varepsilon_b = 0;$$

only the physical root is considered.

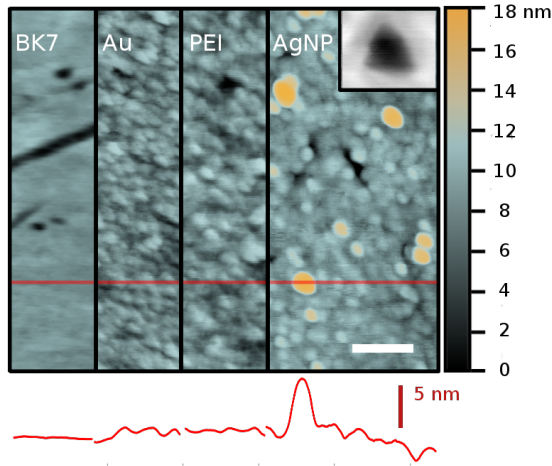


Fig. 5 Combined phase-topography AFM images from individual steps of AgNP deposition; the shown colorbar and 200 nm scale bar are valid for all panels. The inset shows high resolution phase image of a selected AgNP particle with edge length about 60 nm and the height profiles (red) along the marked line in the source topography maps are given in the bottom panel.

Using both nanoscale correction for optical constants of silver (with $v_F = 1.397 \times 10^8 \text{ cm s}^{-1}$ and [26]: $\omega_p = 1.38 \times 10^{16} \text{ s}^{-1}$, $\gamma_{\text{bulk}} = 2.7 \times 10^{13} \text{ s}^{-1}$, $\sigma = 0.75$) and Bruggeman's effective medium, the final simulation of AgNP-modified gold chip sensitivity is summarized in Fig. 6 for several thicknesses of the nanoparticles, each time up to a full monolayer coverage (color maps). The presence of several distinct traces is due to nanoscale correction, while bending of the traces for different mixing ratios is due to effective medium. For each thickness of silver, an optimal thickness of underlying gold can be found that produces strongest resonance. Basically, addition of silver requires thinner underlying gold.

The thickness correction of gold needed in Fig. 6 to achieve optimal resonance with nanoparticles is in agreement with measurements presented in Fig. 4. As anticipated, formula (9) follows the numerical simulation reasonably in the measured range of substrate coverage by the nanoparticles (solid lines). One should emphasize that neither nanoscale correction nor the effective medium have direct effect on the formula (9): the changes manifest through different entering optical constants, not through change of its form.

Although the pronounced shape of the traces in Fig. 6 confirms the need of cautious treatment of Bruggeman's effective medium, a comparison with coherent potential approximation (CPA) shows qualitatively similar results, supporting physical feasibility of the used approximation; for further discussion see Supplement.

To assess the observed variation among different chips, Figure 7 traces measured depth Ψ_{min} of the SPR dip and sensitivity Δ'_{max} for individual steps during preparation of the substrate (dark to light traces). Two generic substrates are shown with area between their traces shaded as a guide to the eye. For optimal readability, the two chips were aligned by their optimal bare gold resonance. Concluding

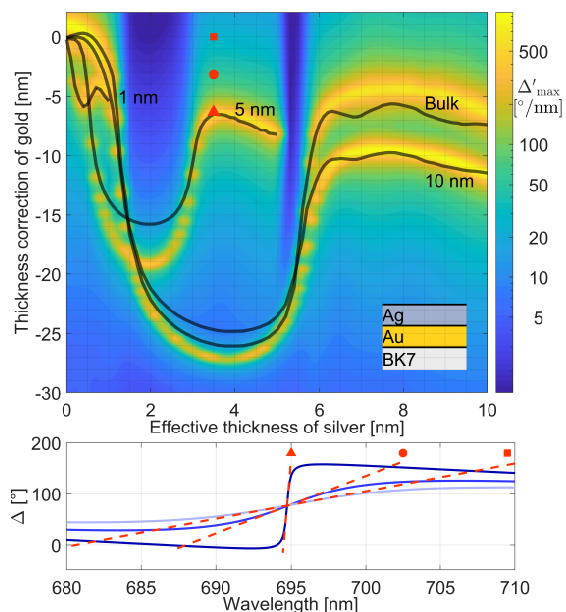


Fig. 6 Model ellipsometric sensitivity of BK7/Au/Ag substrate for AOI= 70° in water ambient using Bruggeman effective medium approach. Dependence of coverage of the substrate with nanoparticles of different size (color maps), including nanoscale correction (1). Analytical approximation (9) for optimal combination of thicknesses based on same optical constants (solid lines).

from the figure, binding of PEI produces changes of SPR dip at the level comparable with chip variability. On the contrary, after coating with silver nanoparticles the resonance diminishes at its original location for bare gold and strengthens in the location originally off resonance to the level comparable with those of bare gold. Consistent with modelling, the best resonance after AgNP immobilization is achieved for a thinner gold layer.

Finally, for routine characterization of the prepared chips, optical spectroscopy is advisable. Although dielectric function of the gold layer is subject to considerable variability (primarily due the grain size and surface roughness [27] of the Au layer), properties of layers created under same conditions tend to be repeatable and the measurement is readily accessible. The X-ray measurement can than be used in role of single-time calibration, such as has been provided in Figs. 7 and 8.

To this end, gold thickness in Fig. 6 is also shown relative to its optimal value before coating with nanoparticles. As such, the figure can be directly used during generic experiment scheduling.

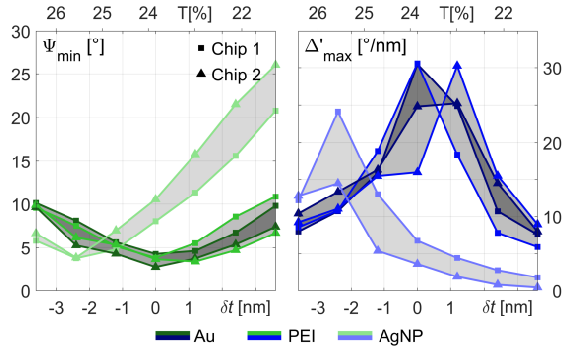


Fig. 7 Measured depth Ψ_{\min} of SPR dip (left panel) and sensitivity Δ'_{\max} (right panel) for the steps in preparation of the BK7/Au/PEI/AgNP substrate from TIRE measurement at AOI= 73° . Data along the gradient of gold are given (dark to light traces) for two generic chips (triangles and squares) aligned (at $\delta t = 0$ nm) by optimal resonance of bare gold. Shading (dark and light) between corresponding traces of the two chips is used as a guide to the eye. The upper horizontal axis displays the measured transmissivity of the gold layer across the chip.

Conclusion

Even a thin silver overlayer has a profound impact on plasmonic resonance of gold substrates. We have provided both theoretical and experimental background for fine-tuning of the SPR using adsorption of the silver nanoparticles. To obtain optimal sensitivity towards subsequent immobilization of biomolecules, the needed thickness decrease of gold layer is quantified by formula (9), however, for quick orientation Fig. 6 may suffice. As demonstrated, correct optical treatment of the silver layer is crucial to reach agreement with measurements.

Although we base our treatment on ellipsometric angle Δ , the results are equally valid in conventional SPR measurements.

Using nanoparticles to tune SPR is motivated by further characterization of the immobilized biomolecules using SPM or (tip or surface enhanced) Raman spectroscopy. The advantage of our method is that it can utilize the well-understood and available gold SPR substrates. In addition, selecting suitable morphology of nanoparticles and controlling the density of their deposition allows for preparation of plasmonic substrates with well controlled resonance properties.

Relying on difference ellipsometric spectra of the substrate, our treatment is valid for all analytes. Despite its simplicity, the used approximation of optical path provides good results for realistic surface coverage by the nanoparticles.

Acknowledgement

Group of dr. Štefl (CEITEC, Masaryk university) is acknowledged for providing the Rtt103 protein.

Funding

This work was supported by the project "CEITEC- Central European Institute of Technology" (CZ.1.05/ 1.1.00/02.0068) from European Regional Development Fund.

Ethical Approval

Not applicable

Consent to Participate

Not applicable

Consent to Publish

Not applicable

Authors Contributions

All authors contributed to the study conception and design. Material preparation, data collection and analysis were performed by J. Dvořák (TIRE, UV-VIS), O. Caha (X-ray) and D. Hemzal (AFM). Simulations were performed by J. Dvořák and nanoparticles were synthesized by D. Hemzal. The first draft of the manuscript was written by D. Hemzal and all authors commented on previous versions of the manuscript. All authors read and approved the final manuscript.

Competing Interests

The authors have no relevant financial or non-financial interests to disclose.

Availability of data and materials

The datasets generated and/or analysed during the current study are available from the corresponding author on reasonable request.

References

1. Maver U., Planišek O., Jamnik J., Hassanien A.I. and Gaberšček M.: *Preparation of Atomically Flat Gold Substrates for AFM Measurements*, Acta chim. slov. **59**(1), 212-219 (2012)
2. Prochazka P., Mach J., Bischoff D. et al: *Ultrasmooth metallic foils for growth of high quality graphene by chemical vapor deposition*, Nanotechnology **25**, 185601 (2014)
3. Homola J.: *Present and future of surface plasmon resonance*, Anal. Bioanal. Chem. **377**(3), 528-539 (2003)

4. Wang Z., Cheng Z., Singh V., Zheng Z., Wang Y., Li S., Song L. and Zhu J.: *Stable and Sensitive Silver Surface Plasmon Resonance Imaging Sensor Using Trilayered Metallic Structures*, Anal. Chem. **86**, 1430-1436 (2013)
5. Chu H-Ch., Kuo Ch-H. and Huang M.h.: *Thermal Aqueous Solution Approach for the Synthesis of Triangular and Hexagonal Gold Nanoplates with Three Different Size Ranges*, Inorg. chem. **45**(2), 808-813 (2006)
6. Deckert-Gaudig T. and Deckert V.: *Ultraflat Transparent Gold Nanoplates - Ideal Substrates for Tip-Enhanced Raman Scattering Experiments*, Small **5**(4), 432-436 (2009)
7. Scaffardi L.B., Lester M., Skigin D. and Tocho J.O.: *Optical extinction spectroscopy used to characterize metallic nanowires*, Nanotechnology **18**, 315402 (2007)
8. Ciesielski A., Skowronski L., Trzcinski M., Szoplik T.: *Controlling the optical parameters of self-assembled silver films with wetting layers and annealing*, Appl. Surf. Sci. **421**(B), 349-356 (2017)
9. Tompkins H.G., Irene E.A., editors: *Handbook of ellipsometry*. Springer, 2005.
10. Arwin H., Poksinski M., Johnsen K.: *Total internal reflection ellipsometry: principles and applications*, Appl. Optics **43**(15): 3028-3036 (2004)
11. Nelson S.G., Johnston K.S., Yee S.S.: *High sensitivity surface plasmon resonance sensor based on phase detection*, Sens. Actuators B 35-36, 187-191 (1996)
12. Hemzal D., Kang Y.R., Dvořák J., Kabzinski T., Kubíček K., Kim Y.D. and Humlíček J.: *Treatment of SPR background in Total internal reflection ellipsometry. Characterization of RNA polymerase II films formation.*, Appl. Spectrosc. **73**(3), 261-270 (2019)
13. Nabok A.V., Tsagorodskaya A. et al: *Total internal reflection ellipsometry and SPR detection of low molecular weight environmental toxins*, Appl. Surf. Sci. (246), 381-386 (2005)
14. Kan Y., Tan Q., Wu G., Si W. and Chen Y.: *Study of DNA absorption on mica surfaces using a surface force apparatus*, Sci. Rep. **5**, 8442 (2015)
15. Jasnovidova O., Klumpler T., Kubicek K., Kalynych S., Plevka P. and Stefl R.: *Structure and dynamics of the RNAPII CTDsome with Rtt103*, PNAS **114**(42), 11133-11138 (2017)
16. Meinhart A., Cramer P.: *Recognition of RNA polymerase II carboxy-terminal domain by 3'-RNA-processing factors*, Nature **430**, 223-226 (2004).
17. Kang T., Niu Y., Jin G.: *Visualization of the interaction between tris and lysozyme with a biosensor based on total internal reflection imaging ellipsometry* Thin Solid Films **571**(3), 463-467 (2014)
18. Bastús N.G., Comenge J. and Puntès V.: *Kinetically Controlled Seeded Growth Synthesis of Citrate-Stabilized Gold Nanoparticles of up to 200 nm: Size Focusing versus Ostwald Ripening*, Langmuir **27**(17), 11098-11105 (2011)
19. Bastús N.G., Merkoçi F. et al: *Synthesis of Highly Monodisperse Citrate-Stabilized Silver Nanoparticles of up to 200 nm: Kinetic Control and Catalytic Properties*, Chem. Mater. **26**(9), 2836-2846 (2014)
20. Cathcart N., Frank A.J., Kitaev V.: *Silver nanoparticles with planar twinned defects: effect of halides for precise tuning of plasmon resonance maxima from 400 to >900 nm*, Chem. Commun., 7170-7172 (2009)
21. Gong H., Garcia-Turiel J., Vasilev K. and Vinogradova O.I.: *Interaction and Adhesion Properties of Polyelectrolyte Multilayers*, Langmuir **21**, 7545-7550 (2005)
22. Feldoto Z., Varga I. and Blomberg E.: *Influence of salt and rinsing protocol on the structure of PAH/PSS polyelectrolyte multilayers*, Langmuir **26**(22), 17048-17057 (2010)
23. Müller M., Meier-Haack J. et al: *Polyelectrolyte Multilayers and their interactions*, J. Adhes. **80**, 521-547 (2004)
24. Palik E.D. (Ed.): *Handbook of optical constants of solids*, New York: Academic Press 1985, Vol 1, pp.286-295
25. Humlíček J.: *Data analysis for nanomaterials: Effective medium approximation, its limits and implementation*, in Losurdo M., Hingerl K. (Eds.): *Ellipsometry at the nanoscale*, Springer (2013)
26. Kreibig U.: *Electronic properties of small silver particles: the optical constants and their temperature dependence*, J. Phys. F: Met. Phys. **4**, 999-1014 (1974)
27. Aspnes D.E., Kinsbron E., Bacon D.D.: *Optical properties of Au: Sample effects*, Phys. Rev. B. **21**(8), 3290-3299 (1980)
28. Suresh A.K., Pelletier D.A., Moon J.-W., Phelps T.J. and Doktycz M.J.: *Size-Separation of Silver Nanoparticles Using Sucrose Gradient Centrifugation*, J. Chromatogr. Sep. Tech. **6**(5), 283 (2015)

Appendix

PVD. The gold layers were prepared by thermal evaporation with thickness gradient along one dimension of 25x25 mm² BK7 microscopy slides using substrate tilting; in particular, tilt angle 57° was used. The transmissivity across the prepared substrates was measured, see Fig. 8, with optimal SPR of bare gold for $T_{\max} = 24\%$.

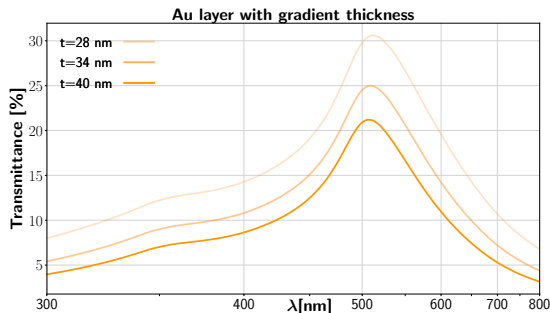


Fig. 8 Transmissivity of Au layer in air ambient (Chip 1 from Fig. 7) at different positions along the thickness gradient; the thicknesses were calibrated using X-ray reflectivity. The maximum transmissivity T_{\max} near $\lambda = 500$ nm can be used to characterize the layers.

PEM. To create a charged surface coating of the SPR chip we use the PEI-PSS-PAH polyelectrolyte multilayer. In particular, 0.1 mg/ mL poly(ethyleneimine) (PEI, M_w 600-1 000 kDa) solution in 150 mM NaCl buffer has been prepared using high purity (>18 M Ω cm) demineralized water and coated on the gold substrates. Consequently, a polyelectrolyte multilayer can be prepared by alternation of 0.1 mg/mL poly(sodium 4-styrenesulfonate) (PSS, negative charge) and 0.1 mg/mL poly(allylamine hydrochloride) (PAH, positive charge), both in 150 mM NaCl buffer.

Rtt103-CID. The stock solution of the used protein (2KM4 structure at rcsb.org) was 1 mM in ITC buffer (35 mM KH₂PO₄, 100 mM KCl, 1 mM BME, pH 6.8). Prior to measurement, the stock solution was diluted 1:100 using DI water.

AgNP. The silver nanoparticles were synthesized according to [20]. In brief, using high purity (>18 M Ω cm) demineralized water (DI), 6 mL of 12.4 mM trisodium citrate dihydrate, 15 mL of 375 μ M AgNO₃, 15 mL of 50 mM H₂O₂, and 10 μ L of 1 mM KBr solutions were prepared and mixed in a clean 50 mL beaker. While stirring the solution, 7.5 mL of 5 mM NaBH₄ were added (all chemicals were used as purchased from Sigma-Aldrich). Stirring for further 10 minutes, the pale yellow solution changed color from yellow through orange and pink to violet and blue. The vials were kept untied for 24 hours to allow sodium borohydride to decompose safely.

The post-synthesis purification of the nanoparticles is an important step in preparing their immobilization. If used as prepared, the synthesis buffer would screen the nanoparticles from binding to the substrate. To prevent this, we employ centrifugation to decrease significantly the concentration of buffer salts, as the used protocol renders stable nanoparticles even after replacement of synthesis

buffer with water. In addition, the centrifugation improves monodispersity of the nanoparticles.

To this end, the nanoparticles were centrifuged prior to use in four steps (10 min at RCF of 5 200 g each). After each step, >99% of supernatant was removed and refluxed with DI to ensure final dilution of the synthesis buffer by at least $1:10^8$. Both the as-synthesized and centrifuged nanoparticles were kept at 10°C , showing stability for over a month at RT.

The purification was monitored through absorbance measurement: as prepared, the nanoparticles show λ_{LSPR} of 608 nm with FWHM 228 nm. After four-step centrifugation, λ_{LSPR} moves to 627 nm and FWHM improves to 187 nm. To study the properties of the nanoparticles in detail, we have performed rate-zonal centrifugation [28], which confirmed presence of NPs with fractionated mass (the upper fractions seen in the inset). The situation is depicted in Fig. 9. Apart from slight shift of λ_{LSPR} to 638 nm, the bottom centrifugate, containing the targeted NPs, shows absorption spectrum equivalent to the one after four-step centrifugation. Consequently, one can safely adhere to the simpler four-step centrifugation suggested here.

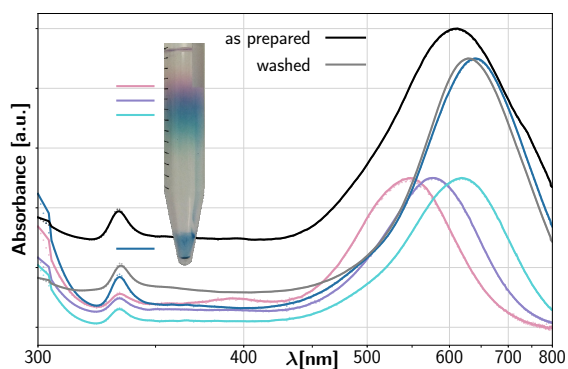


Fig. 9 Absorbance of silver nanoparticles: as prepared, and washed by step centrifugation. The inset shows the result of rate-zonal centrifugation.